This is the accepted manuscript made available via CHORUS. The article has been published as:

Two-dimensional local correlations of octahedral tilts dictate thermal transport in three-dimensional metal halide perovskites

Sandip Thakur and Ashutosh Giri

Phys. Rev. B **111**, 134303 — Published 17 April 2025

DOI: 10.1103/PhysRevB.111.134303

Two-dimensional local correlations of octahedral tilts dictate thermal transport in three-dimensional metal halide perovskites

Sandip Thakur[1] and Ashutosh Giri[1,*]

[1]*Department of Mechanical, Industrial, and Systems Engineering, University of Rhode Island, Kingston, RI 02881, USA*

(Dated: April 9, 2025)

Abstract

In pure nonmetallic crystals, the resistance to heat conduction at temperatures around and above room temperature is conventionally accepted to originate from anharmonic phonon-phonon interactions. Herein, we reveal a different mechanism of heat transfer, which cannot be described by the typical phonon gas picture, where local two-dimensional correlations of the octahedral motions lead to a temperature-independent thermal conductivity (above room temperature and approaching the melting temperature) in $CsPbI_3$. Our systematic atomistic simulations allow us to relate the unique lattice dynamics to the thermal transport in $CsPbI_3$, providing evidence for the indirect (but crucial) role of the Cs^+ ions in facilitating heat transfer at relatively higher temperatures. This contrasts with the conventionally accepted notion of the 'rattling' scenario leading to the reduced thermal conductivities in metal halide perovskites, where the decoupled motion of the Cs^+ ions scatter the acoustic modes of the framework. Rather, we show that the interaction between the Cs^+ ions and the PbI_6 framework enable the local 2D spatiotemporal correlations of the octahedra leading to better heat conduction at higher temperatures in these solids. Our work reveals that local spatiotemporal correlations between atoms, beyond the typical phonon gas picture, can dictate thermal transport in the highly anharmonic metal halide perovskites, and could help guide their further advancements in photovoltaic and thermoelectric applications.

* ashgiri@uri.edu

I. INTRODUCTION

The description of heat conduction in nonmetallic crystals has traditionally been rooted in the widely accepted phonon gas model (PGM),[1–4] in which heat is primarily carried by phonon wave packets with well-defined group velocities.[5] In this description, phonons are treated as gas particles with specific mean free paths, and the intrinsic thermal resistance arises from anharmonic phonon-phonon interactions.[6] This manifests in a sharply decreasing thermal conductivity (κ) with temperature (T), typically at intermediate temperatures where boundary scattering at the sample surface has negligible influence on heat conduction. Experimental measurements of $\kappa(T)$ in this temperature regime have been successfully replicated with the PGM, providing a thorough description of the heat conduction mechanisms in crystals with well separated phonon branches (i.e. where the linewidths are smaller than the interbranch spacings).[7–12] This description, however, has been inadequate for predicting $\kappa(T)$ of highly anharmonic solids with phonon linewidths larger than the interbranch spacings.[13–18] A more recent theoretical model based on the Wigner formulation, incorporating wave-like tunneling of phonons (that are not captured by the traditional PGM), has been utilized to explain the slower decrease in $\kappa(T)$ at intermediate temperatures for such highly anharmonic crystalline solids with ultralow or glass-like κ.[19–23] The formalism has also been applied to explain the plateau in $\kappa(T)$ arising from disorder in several materials with complex unit cells.[24–29]

Although the traditional PGM and the Wigner formulation (along with the combination of the two that provides a unified approach) have been successful in describing $\kappa(T)$ for intermediate temperatures in different types of crystalline solids, these formalisms, that require calculations of instantaneous force constants based on computationally expensive first-principles calculations, are mostly limited to small supercells.[16, 19] As such, these formalisms may not be appropriate for fully describing the heat conduction mechanisms in solids where larger spatial or temporal correlations of the atomic motion (requiring longer simulation times and larger supercell sizes) could be dictating $\kappa(T)$. For instance, utilizing large scale simulations on tens of millions of atoms in molecular dynamics (MD) simulations, a recent work by Thébaud *et al.* showed that long-range spatial correlations in the defect distribution can scatter the low-frequency heat-carrying acoustic modes, leading to a drastic reduction in κ.[30] Here, by utilizing MD simulations on metal halide perovskites (MHPs), we demonstrate a new heat transfer mechanism beyond what can be captured by the typical PGM, where two-dimensional (2D) local correlations of the octahedral motions

dictate $\kappa(T)$ at intermediate and higher temperatures in three-dimensional (3D) MHPs.

In MHPs with the chemical formula ABX_3, many of the physical attributes, including their ultralow thermal conductivities, originate from their unique lattice dynamics; their large anharmonicity is associated with the motion of the corner sharing BX_6^- octahedra with metals at the center and halides at the corners forming a 3D anion cage that host A-site cations. For example, the mechanically soft nature with high degree of spatial fluctuations of the halide ions, resulting in severe anharmonic effects from the dynamic motion of the octahedra,[31] have been shown to be responsible for carrier scattering and the ultralow thermal conductivities in these materials.[32–37] In terms of the understanding of the heat transfer mechanisms in MHPs, several works have shown that the highly anharmonic lattice dynamics renders the heat conduction in MHPs at the intersection of glass-like and crystal-like regimes. For instance, utilizing the Wigner formulation, Simoncelli *et al.*[16] have shown that the thermal transport in $CsPbBr_3$ is governed not only by the particle-like phonon wave packets, but the majority of contribution ($\sim$70% at room temperature) comes from wave-like tunneling of phonons that are not captured by the traditional PGM. Following their work, the Wigner formulation has been applied to show the dominant contribution to κ from wave-like tunneling of phonons in several other lead-free MHPs.[20, 38–40] These works have attributed the high degree of anharmonicity in MHPs to localized modes originating from the 'rattling' dynamics of the A-site cation. In fact, the low energy flat branches associated with the 'rattling' vibrations of the cations inside the perovskite cages is widely believed to drive the ultralow thermal conductivities in MHPs.[16, 32–35, 37, 38, 41, 42]

In the rattling picture, thermal conductivity is mainly limited by the resonant scattering with the rattling modes. The implication in such a picture of thermal transport is that the dynamics of the 'guest' cations inside the nanocages are decoupled from the 'host' framework and serve as additional channels of phonon scattering to the heat carrying acoustic modes of the framework. Such 'rattling' scenarios have been shown to exist in clathrates,[43–46] skutterudites,[47–49] and other compounds with complex unit cells.[18, 50] For MHPs, the evidence for rattling (of the A-site cation inside the octahedral cages), leading to the reduction in κ, has been mainly implied from first-principles calculations of the phonon dispersions showing band crossings (and hybridizations) between acoustic modes of the BX_6 framework and low lying optical modes of the A-site cations.[37, 38, 42] However, it is unclear (from these first-principles calculations) whether the dynamics of the guest cations inside the nanocages are indeed decoupled from that of the 'host' framework – a critical prerequisite for the rattling scenario and the plausible association of

rattling-induced scattering of phonons in dictating the ultralow thermal conductivities in MHPs.

Along with the lack of unequivocal evidence for the rattling picture, prior first-principles calculations have also not been able to entirely take into account the full anharmonicity (beyond the typical three-phonon processes) in MHPs; the higher-order phonon interactions could be crucial in dictating the thermal conductivity of these mechanically soft solids, especially at higher temperatures. Moreover, as mentioned above, these calculations are also mostly limited to small supercell dynamics of the constituent particles around their equilibrium positions and are unable to incorporate any effects from local correlations of octahedral motions that have been recently shown to impact the lattice dynamics of these solids.[51–53]

Here, we utilize systematic MD simulations to unravel the unique temperature-dependent lattice dynamics and thermal transport properties of $CsPbI_3$, the prototypical fully inorganic MHP. We show that, unlike in typical inorganic crystals where thermal conductivity decreases with increasing temperature due to enhanced phonon-phonon scattering, the thermal conductivity of $CsPbI_3$ is independent of temperature at relatively higher temperatures. We attribute this to the enhancement in thermal transport from local 2D correlations in the dynamics of the octahedra at higher temperatures, which is indirectly facilitated by the lattice dynamics of the Cs^+ cations inside the octahedral cages. Through dynamic structure factor calculations based on inelastic neutron scattering (INS), we show that the guest cations are responsible for considerable phonon hardening in $CsPbI_3$, a completely opposite scenario to the widely accepted 'rattling' picture where the motion of the A-site cations are perceived to lower κ in MHPs. These calculations show that the lattice dynamics and thermal conductivity of $CsPbI_3$ at higher temperatures is critically governed by 2D (short-range) structural correlations of the dynamic tilting in the PbI_6 octahedra that are several unit cells wide.

II. METHODS

A. Interatomic potential for $CsPbI_3$ and $SrTiO_3$

To accurately describe the interatomic interactions between the atoms, we use the classical MYP interatomic potential based on first-principles calculations.[54–56] This potential utilizes the Buckingham–Coulombic interatomic potential given by,

$$\Phi = \sum_{\alpha,\beta} \left[A_{\alpha\beta} e^{-r_{\alpha\beta}/\rho_{\alpha\beta}} - \frac{C_{\alpha\beta}}{r_{\alpha\beta}^6} \right] + \sum_{\alpha \neq \beta} \frac{1}{4\pi\epsilon_0} \frac{q_\alpha q_\beta}{r_{\alpha\beta}}. \quad (1)$$

The parameters used to model the pairwise interactions between atoms are given in Table I. The potential has been successfully utilized to reproduce the main static and dynamical properties of methylammonium lead halide perovskites (such as the lattice constants, cohesive energy curves, bulk modulus, and the energy barriers for the rotation of the cations).[54–56] For $CsPbI_3$, the potential is based on our prior work in Ref. [56], where we have shown that the potential is capable of reproducing accurate lattice parameters and the temperature-dependent phase transitions of $CsPbI_3$. Similar interatomic potential has also been utilized by several prior works to study the thermal properties of methylammonium lead halide perovskites.[57–59] Other physical properties, such as the elastic softness,[60–62] vibrational and structural properties,[63] and ionic polarization and mobilities[64] have also been well reproduced with the potential. For $SrTiO_3$, we have implemented a similar interatomic potential developed by Thomas *et al.*,[65] which has been validated against DFT structures, ensuring accurate energy profiles and effectively describing local cation ordering effects.[65, 66] The parameters for $SrTiO_3$ are given in Table II.

Table I. Parameters used to model $CsPbI_3$.[56, 67]

Interaction	A (kcal/mol)	ρ (Å)	C (kcal/mol Å^6)	Ion	Charge
Cs-Cs	18020301	0.174	0	Cs	1.36
Cs-Pb	32010174	0.154	0		
Cs-I	140000	0.360	0	Pb	2.03
Pb-Pb	70359906	0.131	0		
Pb-I	103496	0.321	0	I	-1.13
I-I	22793	0.482	696.95		

Table II. Parameters used to model $SrTiO_3$.[65]

Interaction	A (kcal/mol)	ρ (Å)	C (kcal/mol Å^6)	Ion	Charge
Sr-Sr	40805.856	0.319894	0	Sr	1.84
Ti-O	335932.138	0.197	0	Ti	2.36
O-O	144109.247	0.231	0	O	-1.40

B. Molecular Dynamics (MD) Simulations

To predict the thermal conductivities of $SrTiO_3$ and $CsPbI_3$ structures, we employed MD simulations utilizing the Green-Kubo (GK) formalism. All simulations are conducted using the large-scale atomic/molecular massively parallel simulator (LAMMPS) package.[68]

Initially our computational domains are equilibrated under the Nosé-Hoover thermostat and barostat (NPT ensemble)[69] for 2 ns with a timestep of 0.5 fs, maintaining a constant number of particles, pressure, and temperature at 0 bar. This is followed by further equilibration in the NVT ensemble for 1 ns, where the system's volume and temperature are held constant, with periodic boundary conditions applied. A final equilibration is performed in the NVE ensemble for 1 ns, where the number of particles, volume, and total energy are conserved. Finally, the thermal conductivities are then calculated using the GK formalism within the framework of equilibrium molecular dynamics (EMD) simulations.

In the GK formalism, the thermal conductivity along the x-, y-, and z-directions are determined as,

$$\kappa_{x,y,z} = \frac{1}{k_{\mathrm{B}} V T^2} \int_0^\infty \langle J_{x,y,z}(t) \cdot J_{x,y,z}(0) \rangle dt. \tag{2}$$

Here, t represents time, T and V denote the temperature and volume of the system, respectively, and $\langle J_{x,y,z}(t) \cdot J_{x,y,z}(0) \rangle$ is the heat current autocorrelation function (HCACF), expressed as:[70]

$$\mathrm{J} = \frac{1}{V} \left(\sum_i v_i \epsilon_i + \sum_i \mathrm{S}_i \cdot v_i \right). \tag{3}$$

Here, v_i, ϵ_i, and S_i correspond to the velocity, energy, and stress of atom i. Heat current data are collected every 7 fs during the simulation, followed by integration of the heat current to determine the converged thermal conductivities. The calculations are carried out under the microcanonical ensemble for a total of 5 ns.

C. Dynamic Structure Factor Calculations

To gain insights into the material's atomic-level dynamics, we calculate the dynamic structure factor, $S(\boldsymbol{Q}, E)$, for our perovskite structures using MD simulations. In this technique, molecular dynamics trajectories, $\boldsymbol{r}_i(t)$ are used to compute $S(\boldsymbol{Q}, E)$ according to the following expression:[3, 52, 71–76]

$$S(\boldsymbol{Q}, E) = \left| \sum_{i}^{N} b_i \int exp\left(i\left(\boldsymbol{Q} \cdot \boldsymbol{r}_i(t) - \frac{E}{\hbar} t \right) \right) dt \right|^2 . \quad (4)$$

In this expression, the calculated $S(\boldsymbol{Q}, E)$ is influenced by either X-ray atomic form factors or thermal neutron scattering lengths, depending on the type of scattering. For neutron scattering, the neutron scattering lengths b_i are used, while for X-ray scatterings, b_i is replaced by the atomic form factors $f_i(Q)$. Here, Q represents the magnitude of the momentum transfer vector, $\boldsymbol{Q}$ from the incident beam to the material, E denotes the energy transferred to the system, and N is the total number of atoms within the system.

For the $S(\boldsymbol{Q}, E)$ calculations, we construct the computational domain using cubic $CsPbI_3$ and $SrTiO_3$ structures, each with 5 atoms per unit cell. These are replicated to form a supercell with dimensions of $20 \times 20 \times 15$. The supercell is first equilibrated using the Nosé-Hoover thermostat and barostat (i.e. the NPT ensemble)[69] for 2 ns with a timestep of 0.5 fs, maintaining constant number of particles, pressure, and temperature at 0 bar. Following this, further equilibration is performed under the NVT ensemble for an additional 2 ns, where the volume and temperature are kept constant. Finally, MD simulations are conducted in the microcanonical ensemble (NVE) for 1.5 ns with a 0.5 fs timestep, during which atomic configurations are recorded for the calculation of $S(\boldsymbol{Q}, E)$.

D. Spectral Energy Density (SED) Calculations

We conduct MD simulations using the SED formalism to investigate the phonon mode-specific characteristics of $CsPbI_3$ structures. In this formalism, we apply a Fourier transform to the atomic velocities in order to calculate the average kinetic energy per unit cell as a function of wave vector ($\mathbf{q}$) and frequency (ω), which is expressed as,[77–79]

$$\Phi(\mathbf{q}, \omega) = \frac{1}{4\pi\tau N_T} \sum_{\alpha}^{3} \sum_{b}^{B} m_b \left| \int_0^{\tau} \sum_{n_{x,y,z}}^{N_T} \dot{u}_\alpha \begin{pmatrix} n_{x,y,z} \\ b \end{pmatrix}; t \right) \times exp\left[i\mathbf{q} \cdot \mathbf{r} \begin{pmatrix} n_{x,y,z} \\ 0 \end{pmatrix} - i\omega t \right] dt \right|^2 . \quad (5)$$

Here τ represents the total simulation time, α corresponds to the Cartesian direction, and $n_{x,y,z}$ denotes a unit cell. N_T is the total number of unit cells in the crystal, b is the atomic label in a given unit cell, B is the atomic number in the unit cell, and m_b is the mass of atom b in the unit cell. The term $\dot{u}_\alpha$ represents the velocity in the α-direction at time t, and $\mathbf{r}$ refers to the equilibrium position of each unit cell.

E. Spectral Heat Current Calculations

To determine the contribution of each vibrational mode to the total heat current, we compute the spectral heat current defined as,[80]

$$Q_{j\to i} = \int_0^\infty \frac{d\omega}{2\pi} q_{j\to i}(\omega) \tag{6}$$

where, ω represents the angular frequency, and $q_{j\to i}(\omega)$ is the interparticle spectral heat current, which is defined as,

$$q_{j\to i}(\omega) = 2Re\big[\tilde{K}_{ij}(\omega)\big] \tag{7}$$

Here, the spectral heat current between atoms *i* and *j* is linked to the correlation time between the forces, $\mathbf{F}_{i,j}$ and the velocities, $\mathbf{v}_i$, $\mathbf{v}_j$. $\tilde{K}_{ij}(\omega)$ is the Fourier transform of the auxiliary correlation function, which is defined as,

$$K_{ij}(t_1 - t_2) = \frac{1}{2}\langle \mathbf{F}_{i,j}(t_1) \cdot [\mathbf{v}_i(t_2) + \mathbf{v}_j(t_2)]\rangle \tag{8}$$

In general, $q(\omega)$ is proportional to the correlation between the interatomic forces and the velocities,

$$q_{j\to i}(\omega) \propto \langle \mathbf{F}_{i,j} \cdot (\mathbf{v}_i + \mathbf{v}_j)\rangle. \tag{9}$$

F. Minimum Thermal Conductivity Model

We compare our results to the minimum thermal conductivity model given as,[81]

$$\kappa_{\min} = \left(\frac{\pi}{6}\right)^{1/3} k_{\mathrm{B}} n^{2/3} \sum v_i \left(\frac{T}{\Theta_i}\right)^2 \int_0^{\frac{\Theta_i}{T}} \frac{x^3 e^x}{(e^x - 1)^2} dx. \tag{10}$$

Here, i represents the polarization index, v_i is the speed of sound, $\Theta_i = v_i(\hbar/k_{\mathrm{B}})(6\pi^2 n)^{1/3}$ is the Debye temperature (cut-off frequency for each polarization), k_{B} is the Boltzmann constant, $\hbar$ is the reduced Planck constant, and $x = \Theta_i/T$.

III. RESULTS AND DISCUSSIONS

We begin by comparing the room temperature thermal conductivities of a wide range of ABX_3-perovskites in Fig. 1a. Although these materials have similar atomic arrangements, the thermal

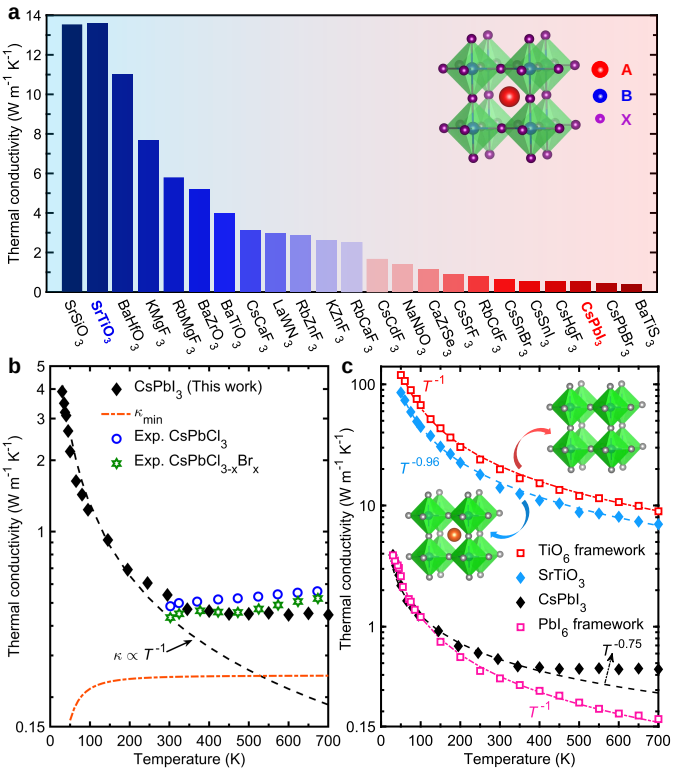


Figure 1. (a) Comparison of room temperature thermal conductivities for different types of ABX_3 perovskites.[34, 37, 82–88] Although they have the same chemical formula, the stiffer oxides have relatively higher thermal conductivities as compared to the mechanically soft halide perovskites. (b) Green-Kubo-predicted temperature dependent thermal conductivity of $CsPbI_3$. The hollow symbols represent the experimental measurements of $\kappa(T)$ on $CsPbCl_3$ and $CsPbCl_{3-x}Br_x$ ($x = 0.01$) single crystal samples.[89] The dashed-dotted line represents the predictions from the minimum thermal conductivity model. At lower temperatures, the thermal conductivity follows a $\kappa \propto T^{-1}$ trend, characteristic of phonon scattering dominated by anharmonic effects. However, as the temperature increases above 300 K, the thermal conductivity of $CsPbI_3$ deviates significantly from the T^{-1} trend, eventually becoming nearly temperature-independent at higher temperatures. (c) Green-Kubo-predicted thermal conductivities as a function of temperature for the stiffer $SrTiO_3$ compared to the softer $CsPbI_3$. We also compare the results to the empty frameworks, where we have removed the A-site cations from the two structures (hollow symbols).

conductivity in these perovskites can vary by more than a factor of forty. This can mainly be attributed to the varying lattice dynamics in the different perovskites. As such, to highlight the unique lattice dynamics associated with $CsPbI_3$, throughout this work, we will compare our results to that of the thermally conductive and mechanically stiff $SrTiO_3$ (the aristotype ABX_3 perovskite).

Our calculations of $\kappa(T)$ for $CsPbI_3$ based on the Green-Kubo approach is shown in Fig. 1b; details of the simulations are provided in the Methods section. For low temperatures ($<$ 200 K), $\kappa(T)$ follows the typical $1/T$ trend, akin to the characteristic behavior of pure crystalline solids.[90, 91] However, $\kappa(T)$ plateaus at a value of $\sim$0.45 W m^{-1} K^{-1} for higher temperatures (even at temperatures approaching the melting point of the solid). We also show the experimental measurements of $\kappa(T)$ for $CsPbCl_3$ and $CsPbCl_{3-x}Br_x$ (x = 0.01) single crystals as carried out by He *et al.*[89] in Fig. 1b. These measurements also demonstrate a temperature-independent thermal conductivity at higher temperatures, where κ remains nearly constant at $\sim$0.55 W m^{-1} K^{-1} across a wide temperature range from 300 to 773 K.[89] This is in line with our MD-predicted thermal conductivity trend at these relatively higher temperatures for $CsPbI_3$.

At the relatively high temperatures shown in Fig. 1b, the thermal conductivity of $CsPbI_3$ is much higher as compared to the hypothetical case where the low temperature $1/T$ trend would continue for higher temperatures. It is interesting to note that this $1/T$ trend would result in ultralow thermal conductivities at high temperatures, which are even lower than the minimum limit to κ for $CsPbI_3$; in the minimum limit the lifetimes of the vibrational modes are limited to half the period of oscillation and heat is conducted through nonpropagating modes.[81] However, we find that $\kappa(T)$ at temperatures around and above room temperature are much higher than the minimum limit of κ for $CsPbI_3$.

As $CsPbI_3$ goes through three structural phase transitions in the temperature range studied in this work, it is important to note that we do not observe any sharp changes in the predicted $\kappa(T)$ (Fig. S9a).[92] $CsPbI_3$ undergoes three structural phases: orthorhombic (*Pbnm*), tetragonal (*P4/mbm*), and cubic ($Pm\bar{3}m$). In the orthorhombic phase, κ follows a power-law decay, $\kappa \propto 1/T^{\alpha}$, with an exponent $\alpha \sim 1$. However, as the structure transitions through the tetragonal and cubic phases, thermal conductivity becomes temperature-independent, suggesting that the conventional phonon-phonon scattering picture alone cannot explain heat transport at relatively higher temperatures in these materials.

The critical role played by the Cs^+ ions in dictating the peculiar $\kappa(T)$ trend becomes clear when we compare the results to the case where we remove the Cs^+ ions from the computational domains (Fig. 1c). For this case, with the nanocages empty, we find that κ follows the $1/T$ trend with reduced κ at higher temperatures as compared to the filled case. This shows that the A-site cations are facilitating heat transfer in this temperature range, which is in contrast to the conventionally accepted notion of 'rattling' of the A-site cations leading to the reduction of κ in MHPs. Even for

filled skutterudites, Li and Mingo have shown that the reduced thermal conductivity is mainly due to increased anharmonic phonon scattering that results from the modification of the entire phonon dispersion through the addition of the filler, ruling out the 'rattling' scenario.[93] Taken together, these observations show that it is instructive to thoroughly analyze the spectral- and mode-level changes introduced by the 'guest' species before associating the low lattice thermal conductivities of many host-guest systems such as MHPs and skutterudites to the 'rattling' scenario.

In Fig. 1c, we compare our results to the calculations for $SrTiO_3$, a relatively stiffer and more thermally conductive perovskite, where the $1/T$ trend does not significantly change for the case with the empty nanocages. Furthermore, in contrast to the case of $CsPbI_3$, with the removal of the Sr^+ ions, we observe an enhancement in thermal conductivity for the TiO_6 framework throughout the entire temperature range. This suggests that the 'rattling' picture is a more appropriate description of heat conduction in the stiffer oxide perovskites.

To further gauge these contrasting results and fully understand the influence of the A-site cations (Sr^+ or Cs^+) on the thermal conductivity, we calculate the INS-based dynamic structure factor, $S(\boldsymbol{Q}, E)$,[3, 52, 71–76] at 300 K for both the filled and empty framework structures (Fig. 2). The variations in the shading intensity of the plots correspond to differing magnitudes of $S(\boldsymbol{Q}, E)$, where brighter regions indicate phonon modes with higher energies. The broadening of peaks in $S(\boldsymbol{Q}, E)$ suggests greater anharmonicity of the modes, stronger phonon-phonon scattering and reduced lifetimes of the vibrational modes. The comparison of $S(\boldsymbol{Q}, E)$ between the filled and empty $SrTiO_3$ structures (Fig. 2a) reveals no significant change in phonon linewidth broadening. However, the acoustic branches are considerably hardened for the case of the empty TiO_6 framework (Fig. 2c). Moreover, the introduction of Sr^+ ions into the TiO_6 framework results in lower group velocities of the acoustic modes. Contrastingly, the INS analysis for $CsPbI_3$ (Fig. 2b) reveals a completely different behavior – the addition of Cs^+ ions within the PbI_6 framework enhances the definition of the wave-vectors for the longitudinal modes, which are notably broadened in the empty framework. Moreover, we observe an increased frequency spectrum for the acoustic modes, where these modes are considerably hardened as compared to the empty PbI_6 framework (Fig. 2d). This shows that the presence of Cs^+ ions leads to higher group velocities and concomitantly higher thermal conductivities at relatively higher temperatures compared to the empty PbI_6 framework (Fig. 1c). Taken together, our comparison of the $S(\boldsymbol{Q}, E)$ calculations for the empty and filled structures emphasize the varying impact of A-site cations on the lattice dynamics and thermal transport in rigid and soft perovskites; while 'rattling' affects κ of the stiffer $SrTiO_3$, for

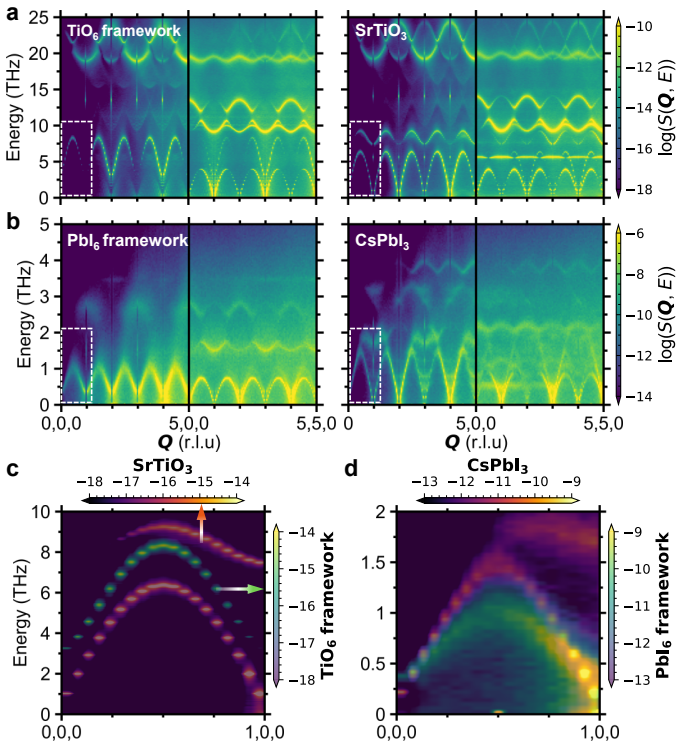


Figure 2. Inelastic neutron scattering dynamic structure factor, $S(\boldsymbol{Q}, E)$ calculated at 300 K for (a) the empty TiO_6 framework and $SrTiO_3$, and (b) the empty PbI_6 framework and $CsPbI_3$. The $S(\boldsymbol{Q}, E)$ calculations are shown along the [1, 0, 0] and [1, 1, 0] directions in the reciprocal space. (c) A magnified view of the highlighted regions in (a) shows a reduced frequency spectrum of acoustic modes in $SrTiO_3$ compared to the empty TiO_6 framework, resulting in lower group velocities and, consequently, lower thermal conductivities for $SrTiO_3$. (d) Contrastingly, a magnified view of the highlighted regions in (b) shows an increased frequency spectrum of acoustic modes in $CsPbI_3$ compared to the empty PbI_6 framework, leading to higher group velocities and, consequently, higher thermal conductivities for $CsPbI_3$.

the softer $CsPbI_3$, the dynamics of the A-site cations facilitates heat transfer. We note here that the contributions to $\kappa(T)$ directly from the Cs^+ ions is negligible and the heat current is totally driven by the PbI_6 octahedra (see Fig. S10).[92]

Next, to comprehensively understand the influence of the octahedral lattice dynamics on the thermal transport in $CsPbI_3$, we calculate the total neutron diffuse scattering, $S(\boldsymbol{Q})$, which can provide insights into the local spatial correlations of the atomic motions. Typically, in a well-ordered crystal, elastic scattering is characterized by sharp Bragg peaks located at the center of the Brillouin Zone, such as in the (HK0) plane for integer values of L (see Fig. S15[92]). Unlike for $SrTiO_3$, where only sharp peaks corresponding to the superstructure of the cubic lattice are ob-

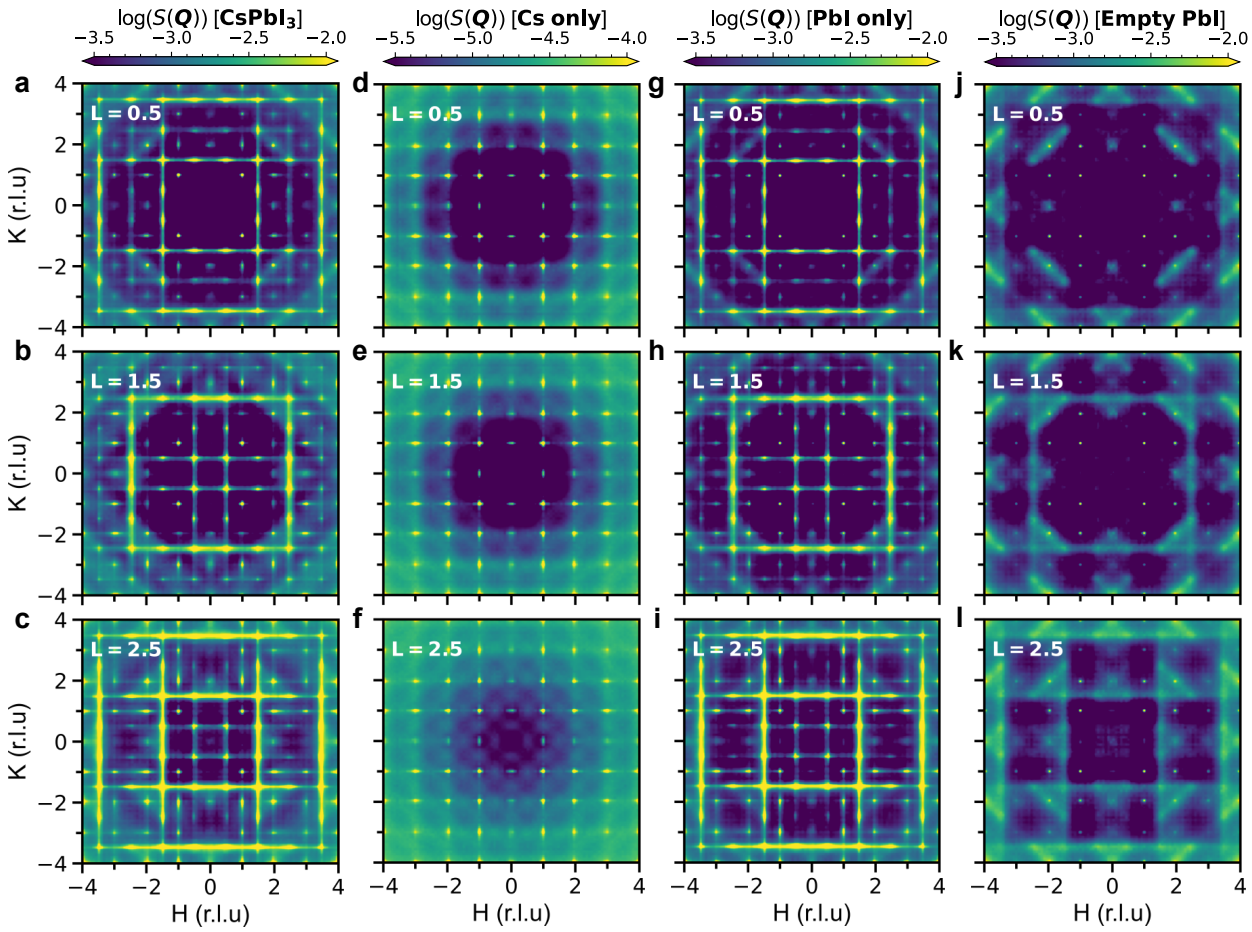


Figure 3. (a-c) Calculated total neutron diffuse scattering, $S(\boldsymbol{Q})$ for $CsPbI_3$ at 600 K, for reciprocal space slices at L = 0.5, 1.5, and 2.5 planes. Contributions to the total neutron diffuse scattering from (d-f) only Cs^+ ions, (g-i) PbI_6 cage, and (j-l) empty PbI_6 framework.

served in the L = 0.5, 1.5, and 2.5 planes (see Fig. S16[92]), the $S(\boldsymbol{Q})$ for $CsPbI_3$ at 600 K, shown in Figs. 3a-c, reveals the presence of distinctly extended diffuse rods spanning the edges of the Brillouin Zone. These rods are broad, isotropic, and exhibit well-defined characteristics, indicative of 2D structural correlations (that are short-range and several unit cells wide) within real space. These correlations manifest as plate-like domains of octahedral frameworks perpendicular to the rods.[94] Similar 2D dynamic structural correlations were observed in $CsPbBr_3$, driven by soft, overdamped, and anharmonic phonons at the Brillouin Zone edge.[51] The presence of such dynamic structural correlations is closely associated with local disorder and polymorphism in halide perovskites, where thermal fluctuations and anharmonic interactions govern phase stability,[95] structural distortions,[95–97] and modulate the material's electronic properties.[96, 97]

We separate the contributions from Cs^+ ions (Figs. 3d-f), and PbI_6 octahedra (Figs. 3g-i) to the

total $S(\boldsymbol{Q})$, and compare with the calculations for the empty PbI_6 framework case (Figs. 3j-l). The $S(\boldsymbol{Q})$ contribution from Cs^+ ions exhibit broad and spherical components indicative of uncorrelated disorder. Contrastingly, the PbI_6 cage shows clear and distinct diffuse rods that highlight the 2D structural correlations of PbI_6 octahedra. Notably, these extended diffuse rods disappear when the Cs^+ ions are removed, as seen in the case of the empty PbI_6 framework (Figs. 3j-l). This highlights the critical role of Cs^+ ions in establishing these local 2D correlations of the octahedra in $CsPbI_3$, which give rise to plate-like domains perpendicular to the diffuse rods.[51, 52, 94]

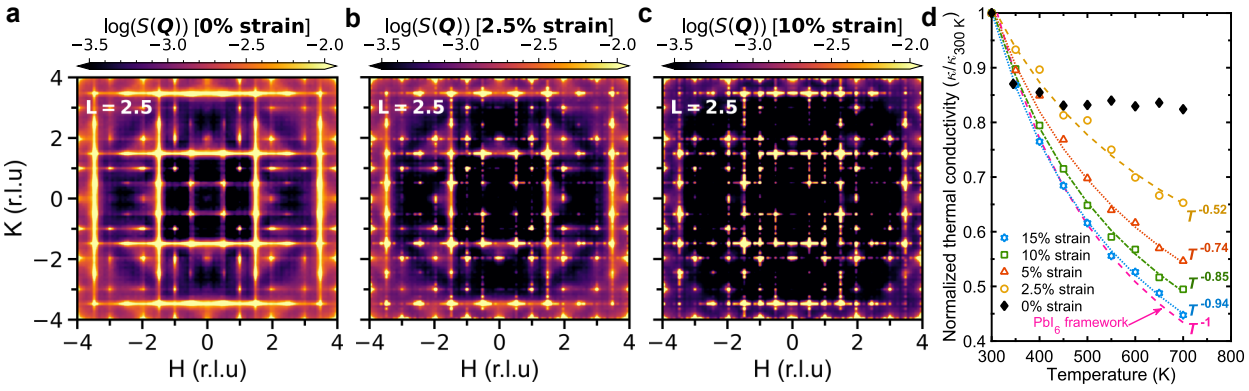


Figure 4. Comparison of calculated total neutron diffuse scattering, $S(\boldsymbol{Q})$ for $CsPbI_3$ at 600 K, for reciprocal space slice at L = 2.5 plane for (a) 0%, (b) 2.5%, and (c) 10% hydrostatic compressions. As strain levels increase, the extended diffuse rods diminish. (d) Comparison of normalized thermal conductivities (relative to the thermal conductivity at 300 K) as a function of temperature for $CsPbI_3$ structures under 0%, 2.5%, 5%, 10%, and 15% hydrostatic compressions. With increasing strain levels, the temperature dependence of the thermal conductivity increases at higher temperatures.

To provide evidence for this hypothesis, we restrict the motion of the octahedra and reduce the free space volume available for the motion of the Cs^+ ions by shrinking the nanocage volume via hydrostatic pressures. Doing so leads to the gradual disappearance of the diffuse rods with increasing strain levels as shown in Figs. 4a-c and S19.[92] The disappearance of the rods indicates that the 2D local correlations are suppressed with increasing hydrostatic strain levels. To understand the influence of the reduced short-range correlations on the thermal transport, we compare $\kappa(T)$ of $CsPbI_3$ under the different levels of hydrostatic compressions and show the normalized $\kappa(T)$ with respect to the room temperature values of the respective strain levels in Fig. 4d. We find that as the strain levels are increased, the plateau in $\kappa(T)$ at higher temperatures for the unstrained $CsPbI_3$ gradually changes to a $1/T$ trend. Combined with the disappearance of the diffuse rods, we

can infer that the local 2D correlations dictate the plateau in $\kappa(T)$ for MHPs at relatively higher temperatures. Moreover, there is a direct correlation between the width of the diffuse scattering rods and $\kappa(T)$; we find that the exponent describing the temperature dependence, α (in $\kappa \propto 1/T^{\alpha}$), monotonically increases to a value of $\sim$1, as the width of the diffuse scattering rods decreases (Fig. S20).[92] This highlights the significant role of polymorphic domain sizes in modulating the temperature dependence of thermal conductivity in these materials. We note that the interatomic potential used in this study has been specifically refined to accurately reproduce the total energy of lead halide perovskites under hydrostatic deformation while also effectively capturing the energy landscapes associated with A-site cation reorientation within the deforming framework.[54] Furthermore, we observe that applying hydrostatic compression of up to 15% at 600 K does not induce a structural phase transition, and the average symmetry of the system remains cubic. However, it is important to note that this does not imply the formation of a truly ordered cubic phase, as the octahedra remain locally tilted, albeit with reduced dynamic fluctuations under pressure (consistent with prior experimental findings).[98–101]

So far, we have considered the crucial role of the A-site cation and the 2D octahedral correlations on dictating $\kappa(T)$ of $CsPbI_3$. Next, we focus on the temperature-dependent changes to the vibrational spectrum and the phonon dispersion of $CsPbI_3$. For this purpose, we first calculate the phonon spectral energy densities (SEDs), which can inherently incorporate anharmonic effects and provide temperature renormalized phonon dispersions.[77, 78] Figure 5 shows our calculations at three different temperatures providing direct evidence of the anharmonic nature of the solid. SEDs provide key insights into phonon dynamics by revealing phonon dispersion characteristics, where variations in shading intensity correspond to the magnitude of the SED, indicating the relative kinetic energy of vibrational modes. Therefore, the broadening of SEDs indicates increased anharmonicities, stronger phonon-phonon scattering, and reduced phonon lifetimes.[77, 78] With increasing temperature, we observe a significant broadening of the SED peaks, indicating an increase in anharmonicity and stronger phonon-phonon scattering. However, despite this increased scattering, the phonon frequencies and the slopes of the longitudinal and transverse acoustic branches remain largely unchanged. Consequently, the extracted longitudinal ($v_L \sim 2050$ m s^{-1}) and transverse ($v_T \sim 1050$ m s^{-1}) group velocities show negligible variation across all three temperatures. However, it is evident that the coupling of the acoustic modes with the low-lying optical modes increases with increasing temperature, which helps explain the low room-temperature thermal conductivity of $CsPbI_3$.

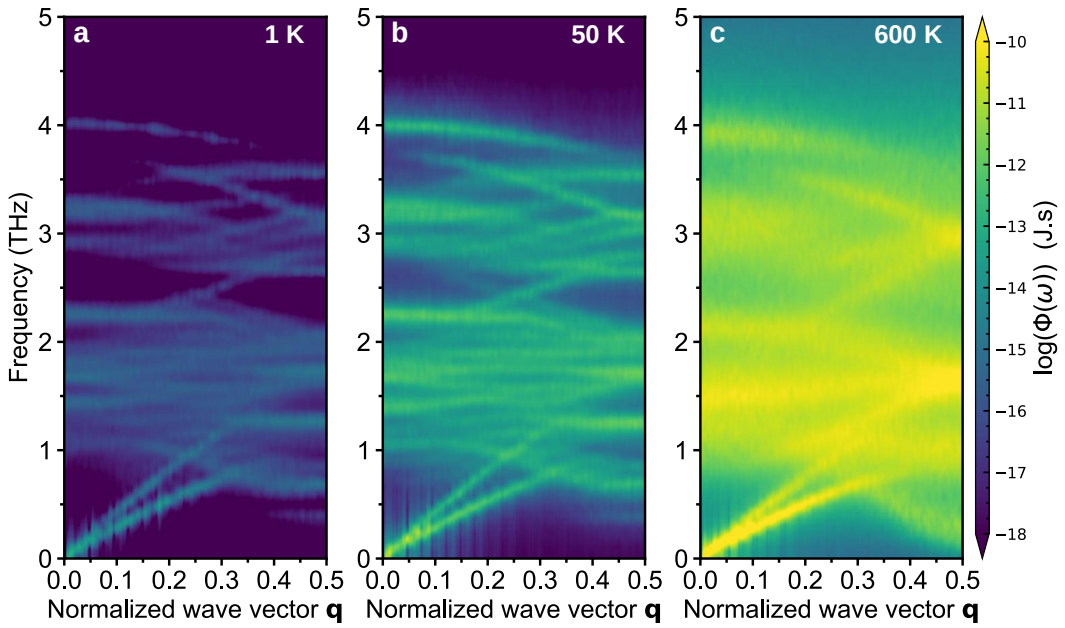


Figure 5. Calculated phonon spectral energy densities (SEDs) for $CsPbI_3$ at (a) 1 K, (b) 50 K, and (c) 600 K. The shading represents the magnitude of the SED. The broadening of SED peaks with increasing temperature indicates enhanced anharmonicity, stronger phonon-phonon scattering, and reduced phonon lifetimes. However, despite this increased anharmonicity, the phonon frequencies and the slopes of the longitudinal and transverse acoustic branches remain largely unchanged. This suggests that the temperature-induced phonon broadening (and renormalization) in $CsPbI_3$ is primarily leading to an increase in phonon scattering rates rather than changes in acoustic phonon group velocities.

We now attempt to provide a simple analytical model that could help describe the influence of the 2D spatial correlations of the octahedral tilts in dictating $\kappa(T)$ for $CsPbI_3$. In Ref. [56], a similar anomalous temperature trend was predicted for $MAPbI_3$, which was described by the sum of two terms, which includes a term that decreases with temperature (akin to the temperature dependence of crystals, where anharmonic phonon-phonon scattering dominates) and an Arrhenius-like term (where an energy barrier, E_b, controls the temperature dependence) given as,

$$\kappa(T) = (\frac{T_1}{T})^u + e^{-E_b/k_B T}(\frac{T}{T_2})^c. \tag{11}$$

Here k_B is the Boltzmann constant and T_1, T_2, u, and c are fitting parameters. The fitting to the $\kappa(T)$ of $CsPbI_3$ yields $u \sim 1$ and $E_b \sim 16$ meV (see Fig. 6). In Ref. [56], the model fitting for $MAPbI_3$ (as shown in Fig. 6) provided an $E_b \sim 30$ meV, which was prescribed to the activation energy of the molecular rotations. Our extracted value of E_b for $CsPbI_3$ is comparatively lower

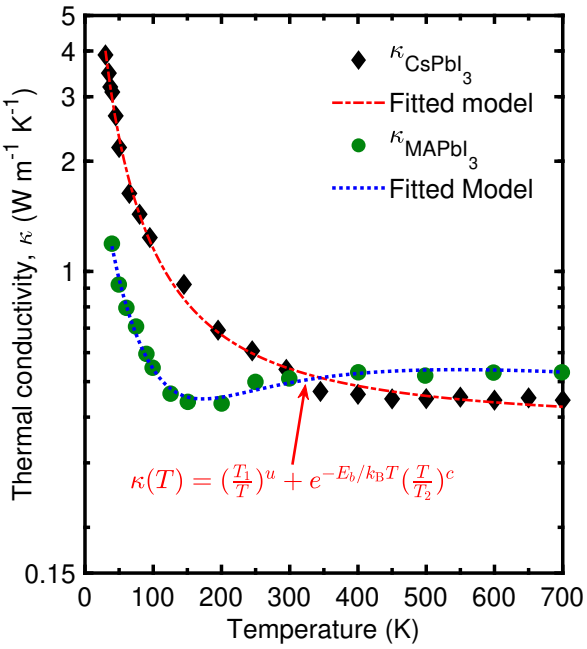


Figure 6. Thermal conductivity as a function of temperature for $CsPbI_3$ and $MAPbI_3$ (taken from Ref. [56]). The dashed-dotted and dotted lines represent fits to $\kappa(T)$ using the model: $\kappa(T) = (\frac{T_1}{T})^u + e^{-E_b/k_B T}(\frac{T}{T_2})^c$. The first term describes a power-law decay of κ with temperature, while the second term accounts for an Arrhenius-type activated process. The extracted energy barrier is $E_b \sim 16$ meV for $CsPbI_3$ and $E_b \sim 30$ meV for $MAPbI_3$. Notably, for $CsPbI_3$, E_b is significantly lower than the activation energy required for molecular rotations in hybrid perovskites.

than the activation energy of the cation rotations in hybrid MHPs.[54, 102, 103] It should be noted that similar 2D octahedral correlations have also been demonstrated in $MAPbI_3$ computational domains modeled with the MYP potential.[52] Thus, the higher activation energy barrier in the case of $MAPbI_3$ might be expected since both the 2D correlations and the rotations of the organic cations add 'disorder' to the system.

To investigate the relationship between the activation energy and phase transitions, we perform nudged elastic band (NEB) calculation, which is a widely used technique for identifying the minimum energy path and the corresponding energy barrier between two states.[104, 105] Our calculations yield an energy barrier of $\sim$33 meV for the activation of the octahedral tilts (see Fig. S21), which is consistent with prior works that have considered the activation energy for the tilts.[106, 107] This value is twice the activation energy extracted from the fit to $\kappa(T)$. However, it is important to note that the $\sim$16 meV value represents the energy barrier for the dynamic 2D correlations of octahedral tilts (as opposed to the activation of the tilts).

The dynamic disorder originating from the highly anharmonic nature in the lead-based hybrid and fully inorganic perovskites results in their peculiar temperature dependence (or the lack thereof) of thermal conductivity at relatively higher temperatures. Although not yet demonstrated for a range of MHPs, it could be expected that the highly anharmonic nature of these materials (in general) could lead to the peculiar temperature-independent $\kappa(T)$ at higher temperatures for a wider range of MHPs. As such, our work advocates the need for further studies where experimental measurements at higher temperatures are combined with atomistic simulations based on accurate interatomic potentials to provide insights into the thermal transport properties of different MHPs.

It should be pointed out that the plateau in $\kappa(T)$ for several complex unit cell crystals has been described more rigorously with the recently developed Wigner formulation, which accounts for the contributions from the wave-like interbranch tunnelling between phonon modes.[16, 19] These contributions from the non-propagating (diffuson) modes are shown to increase with temperature, and can even become the dominant mechanism of heat conduction at higher temperatures. In fact, Simoncelli *et al.* have shown that in $CsPbBr_3$ at room temperature, the particle-like phonon transport has a minor contribution with just 30% of the total thermal conductivity while the contributions from the wave-like tunneling provides the dominant 70% contribution.[16] Such a description is beyond the typical PGMs based on three-phonon scattering, which predict a $1/T$ trend for crystalline solids.[12] Inclusion of higher-order phonon scattering processes (such as quartic phonon-phonon interactions) can change this temperature trend in solids, especially at higher temperatures where these higher-order processes can be important.[108–110] However, to explain the temperature independence (or the plateau) of thermal conductivity at higher temperatures for highly anharmonic crystals requires a unified approach (such as the Wigner formalism)[16, 19] that can fully account for the particle-like phonon-phonon scattering processes and the contributions from the wave-like tunneling between vibrational eigenstates.

The 2D correlations of the octahedral tilts in the halide perovskites have been shown to be dynamic in both space and time,[51, 53, 111] thus requiring large supercell sizes and long simulation times. These layered correlations (that are a few unit cells thick) are shown to be extended over the entire plane and occur dynamically over long timescales.[51, 53, 111] In such a case, MD simulations might be well-poised since they can account for such longer spatiotemporal correlations and intrinsically incorporate higher-order phonon interactions. Although such short-range local correlations of the atoms dictating the thermal transport properties has yet to be revealed in other

crystalline solids, our work advocates for a unified *ab initio*-based approach that can capture the contributions of (short-range) local correlations in the lattice dynamics of the atoms and the coupling mechanism between such correlations and the phonons. Similarly, experimental evidence of such a phenomenon requires accurate measurements of the thermal conductivity of diverse MHPs at relatively higher temperatures and preferably going up-to the melting temperature of the solid.

Finally, we emphasize that our results add to the recent body of works that have shown that the thermal transport in these materials is at the intersection of crystal-like and glass-like regimes.[16, 35, 38, 112, 113] The increasing thermal conductivity at low temperatures suggests anharmonic scattering (akin to pure crystalline semiconductors) dictates the low-temperature dependence, whereas the plateau at higher temperatures suggests a more glass-like trend in this regime. While thermal transport in the PGM for crystals is dictated by the scattering mechanisms of phonons that have plane wave characteristics and well-defined phase and group velocities, in glasses, non-propagating vibrational modes (that do not possess plane wave characteristics) dominate heat conduction. This prompted Allen and Feldman to propose a taxonomy of vibrational heat carriers that exist and transfer energy at different length scales in amorphous solids.[13, 114] In this refined picture, three classes of vibrational modes exist: i) propagating, phonon-like delocalized modes (propagons); ii) non-propagating, delocalized modes (diffusons); and iii) non-propagating, localized modes (locons). For glasses, the harmonic coupling between the non-propagating (diffuson) modes, which arises from the off-diagonal elements of the velocity operator, increases with temperature. The Wigner formalism mentioned above seamlessly integrates the particle-like phonon scattering and the diffuson contributions from the off-diagonal term, providing a unified approach to model the thermal conductivity of both glasses and crystals.[16, 19] In this regard, for our MHPs, it could be that the dynamic 2D correlations potentially alter not only the dynamics of propagating modes but also influence (and facilitate) the diffusonic processes in these materials leading to higher contributions at the relatively higher temperatures. Insights into the coupling of such intrinsic lattice dynamics (that varies over space and time) and the intrinsic vibrational physics of the material could reveal novel phonon transport processes yet to be realized. For this purpose, with their large range of selections for the choices of the ABX_3 constituents, MHPs provide the ideal materials platform for unraveling and comprehensively understanding such phenomena.

IV. CONCLUSION

In summary, we have systematically explored the lattice dynamics and thermal transport properties of $CsPbI_3$ through a combination of MD simulations and inelastic and diffuse neutron scattering calculations. Our findings reveal a unique temperature-independent thermal transport regime at relatively higher temperatures, primarily driven by local 2D correlations of the octahedra. We have shown that these local correlations, that facilitates heat conduction at relatively higher temperatures, are a consequence of the interactions of the A-site cations with the octahedra. Therefore, even though the Cs^+ ions do not directly affect the heat current, they are indirectly responsible in dictating $\kappa(T)$ of MHPs. This is a completely different mechanism than the conventionally accepted picture of 'rattling' where the vibrational modes associated with the Cs^+ ions are believed to scatter the low frequency acoustic modes, providing resistance to heat transfer in these solids. Our results reveal a new heat transfer mechanism in MHPs that can not be described with the conventional phonon gas models, paving the way for a comprehensive understanding of the structure-property relationships in these highly anharmonic solids.

ACKNOWLEDGMENTS

This work is supported by the Office of Naval Research, Grant No. N00014-24-1-2419.

REFERENCES

[1] R. Peierls, Zur kinetischen theorie der wärmeleitung in kristallen, Annalen der Physik **395**, 1055 (1929).

[2] G. Srivastava, Phonon conductivity of insulators and semiconductors, Journal of Physics and Chemistry of Solids **41**, 357 (1980).

[3] M. T. Dove, *Introduction to lattice dynamics*, 4 (Cambridge university press, 1993).

[4] G. Chen, *Nanoscale energy transport and conversion: a parallel treatment of electrons, molecules, phonons, and photons* (Oxford university press, 2005).

[5] R. J. Hardy, Energy-flux operator for a lattice, Physical Review **132**, 168 (1963).

[6] J. M. Ziman, *Electrons and phonons: the theory of transport phenomena in solids* (Oxford university press, 2001).

[7] J. Garg, N. Bonini, B. Kozinsky, and N. Marzari, Role of disorder and anharmonicity in the thermal conductivity of silicon-germanium alloys: A first-principles study, Physical review letters **106**, 045901 (2011).

[8] D. A. Broido, M. Malorny, G. Birner, N. Mingo, and D. Stewart, Intrinsic lattice thermal conductivity of semiconductors from first principles, Applied Physics Letters **91** (2007).

[9] K. Esfarjani, G. Chen, and H. T. Stokes, Heat transport in silicon from first-principles calculations, Physical Review B—Condensed Matter and Materials Physics **84**, 085204 (2011).

[10] M. N. Luckyanova, J. Garg, K. Esfarjani, A. Jandl, M. T. Bulsara, A. J. Schmidt, A. J. Minnich, S. Chen, M. S. Dresselhaus, Z. Ren, *et al.*, Coherent phonon heat conduction in superlattices, Science **338**, 936 (2012).

[11] D. G. Cahill, P. V. Braun, G. Chen, D. R. Clarke, S. Fan, K. E. Goodson, P. Keblinski, W. P. King, G. D. Mahan, A. Majumdar, H. J. Maris, S. R. Phillpot, E. Pop, and L. Shi, Nanoscale thermal transport. ii. 2003–2012, Applied physics reviews **1**, 011305 (2014).

[12] A. J. McGaughey, A. Jain, H.-Y. Kim, and B. Fu, Phonon properties and thermal conductivity from first principles, lattice dynamics, and the boltzmann transport equation, Journal of Applied Physics **125**, 011101 (2019).

[13] P. B. Allen and J. L. Feldman, Thermal conductivity of disordered harmonic solids, Physical Review B **48**, 12581 (1993).

[14] X. Chen, A. Weathers, J. Carrete, S. Mukhopadhyay, O. Delaire, D. A. Stewart, N. Mingo, S. N. Girard, J. Ma, D. L. Abernathy, *et al.*, Twisting phonons in complex crystals with quasi-one-dimensional substructures, Nature communications **6**, 6723 (2015).

[15] H. R. Seyf, L. Yates, T. L. Bougher, S. Graham, B. A. Cola, T. Detchprohm, M.-H. Ji, J. Kim, R. Dupuis, W. Lv, and A. Henry, Rethinking phonons: The issue of disorder, npj Computational Materials **3**, 1 (2017).

[16] M. Simoncelli, N. Marzari, and F. Mauri, Unified theory of thermal transport in crystals and glasses, Nature Physics **15**, 809 (2019).

[17] L. Isaeva, G. Barbalinardo, D. Donadio, and S. Baroni, Modeling heat transport in crystals and glasses from a unified lattice-dynamical approach, Nature communications **10**, 1 (2019).

[18] S. Mukhopadhyay, D. S. Parker, B. C. Sales, A. A. Puretzky, M. A. McGuire, and L. Lindsay, Two-channel model for ultralow thermal conductivity of crystalline Tl_3VSe_4, Science **360**, 1455 (2018).

[19] M. Simoncelli, N. Marzari, and F. Mauri, Wigner formulation of thermal transport in solids, Physical Review X **12**, 041011 (2022).

[20] J. Zheng, C. Lin, C. Lin, G. Hautier, R. Guo, and B. Huang, Unravelling ultralow thermal conductivity in perovskite cs2agbibr6: dominant wave-like phonon tunnelling and strong anharmonicity, Npj Computational Materials **10**, 30 (2024).

[21] Z. Tong, A. Pecchia, C. Yam, T. Dumitrica, and T. Frauenheim, Glass-like transport dominates ultralow lattice thermal conductivity in modular crystalline bi4o4secl2, Nano letters **23**, 9468 (2023).

[22] Y. Wu, Y. Chen, Z. Fang, Y. Ding, Q. Li, K. Xue, H. Shao, H. Zhang, and L. Zhou, Ultralow lattice thermal transport and considerable wave-like phonon tunneling in chalcogenide perovskite bazrs3, The Journal of Physical Chemistry Letters **14**, 11465 (2023).

[23] J. Li, L. Wei, Z. Ti, L. Ma, Y. Yan, G. Zhang, and P.-F. Liu, Wavelike tunneling of phonons dominates glassy thermal conductivity in crystalline cs 3 bi 2 i 6 cl 3, Physical Review B **108**, 224302 (2023).

[24] A. F. Harper, K. Iwanowski, W. C. Witt, M. C. Payne, and M. Simoncelli, Vibrational and thermal properties of amorphous alumina from first principles, Physical Review Materials **8**, 043601 (2024).

[25] H. Zhou, J. Tiwari, and T. Feng, Understanding the flat thermal conductivity of la 2 zr 2 o 7 at ultrahigh temperatures, Physical Review Materials **8**, 043804 (2024).

[26] A. Pazhedath, L. Bastonero, N. Marzari, and M. Simoncelli, First-principles characterization of thermal conductivity in la po 4-based alloys, Physical Review Applied **22**, 024064 (2024).

[27] Q.-Y. Xie, F. Xiao, K.-W. Zhang, and B.-T. Wang, Anharmonic phonon self-energy and anomalous thermal transport in the quaternary compound baa g 2 sns e 4, Physical Review B **110**, 045203 (2024).

[28] R. Cheng, Z. Zeng, C. Wang, N. Ouyang, and Y. Chen, Impact of strain-insensitive low-frequency phonon modes on lattice thermal transport in a 2 xb 6-type perovskites, Physical Review B **109**, 054305 (2024).

[29] J. Tiwari and T. Feng, Accurate prediction of thermal conductivity of al 2 o 3 at ultrahigh temperatures, Physical Review B **109**, 075201 (2024).

[30] S. Thébaud, L. Lindsay, and T. Berlijn, Breaking rayleigh's law with spatially correlated disorder to control phonon transport, Physical Review Letters **131**, 026301 (2023).

[31] D. A. Egger, A. Bera, D. Cahen, G. Hodes, T. Kirchartz, L. Kronik, R. Lovrincic, A. M. Rappe, D. R. Reichman, and O. Yaffe, What remains unexplained about the properties of halide perovskites?, Advanced Materials **30**, 1800691 (2018).

[32] A. Pisoni, J. Jacimovic, O. S. Barisic, M. Spina, R. Gaál, L. Forró, and E. Horváth, Ultra-low thermal conductivity in organic–inorganic hybrid perovskite $CH_3NH_3PbI_3$, The journal of physical chemistry letters **5**, 2488 (2014).

[33] B. Li, Y. Kawakita, Y. Liu, M. Wang, M. Matsuura, K. Shibata, S. Ohira-Kawamura, T. Yamada, S. Lin, K. Nakajima, and S. F. Liu, Polar rotor scattering as atomic-level origin of low mobility and thermal conductivity of perovskite $CH_3NH_3PbI_3$, Nature communications **8**, 1 (2017).

[34] W. Lee, H. Li, A. B. Wong, D. Zhang, M. Lai, Y. Yu, Q. Kong, E. Lin, J. J. Urban, J. C. Grossman, and P. Yang, Ultralow thermal conductivity in all-inorganic halide perovskites, Proceedings of the National Academy of Sciences **114**, 8693 (2017).

[35] T. Zhu and E. Ertekin, Mixed phononic and non-phononic transport in hybrid lead halide perovskites: Glass-crystal duality, dynamical disorder, and anharmonicity, Energy & Environmental Science **12**, 216 (2019).

[36] A. Ferreira, A. Létoublon, S. Paofai, S. Raymond, C. Ecolivet, B. Rufflé, S. Cordier, C. Katan, M. I. Saidaminov, A. Zhumekenov, O. Bakr, J. Even, and P. Bourges, Elastic softness of hybrid lead halide perovskites, Physical Review Letters **121**, 085502 (2018).

[37] H. Xie, S. Hao, J. Bao, T. J. Slade, G. J. Snyder, C. Wolverton, and M. G. Kanatzidis, All-inorganic halide perovskites as potential thermoelectric materials: Dynamic cation off-centering induces ul-

tralow thermal conductivity, Journal of the American Chemical Society **142**, 9553 (2020).

[38] T. Pandey, M.-H. Du, D. S. Parker, and L. Lindsay, Origin of ultralow phonon transport and strong anharmonicity in lead-free halide perovskites, Materials Today Physics **28**, 100881 (2022).

[39] Q. Wang, Z. Zeng, P. Zhao, C. Chen, N. Ouyang, J. Mao, and Y. Chen, B-site columnar-ordered halide double perovskites: Breaking octahedra motions induces strong lattice anharmonicity and thermal anisotropy, Chemistry of Materials **35**, 1633 (2023).

[40] J.-J. Ma, J.-J. Zheng, Y. Chen, Q. Ren, J. Zhang, and B. Wang, Intrinsic ultralow lattice thermal conductivity in lead-free halide perovskites cs3bi2x9 (x= br, i), Physical Chemistry Chemical Physics **26**, 21801 (2024).

[41] P. Acharyya, T. Ghosh, K. Pal, K. S. Rana, M. Dutta, D. Swain, M. Etter, A. Soni, U. V. Waghmare, and K. Biswas, Glassy thermal conductivity in cs3bi2i6cl3 single crystal, Nature communications **13**, 5053 (2022).

[42] A. Bhui, T. Ghosh, K. Pal, K. Singh Rana, K. Kundu, A. Soni, and K. Biswas, Intrinsically low thermal conductivity in the n-type vacancy-ordered double perovskite Cs_2SnI_6: octahedral rotation and anharmonic rattling, Chemistry of Materials **34**, 3301 (2022).

[43] T. Takabatake, K. Suekuni, T. Nakayama, and E. Kaneshita, Phonon-glass electron-crystal thermoelectric clathrates: Experiments and theory, Reviews of Modern Physics **86**, 669 (2014).

[44] G. Nolas, J. Cohn, G. Slack, and S. Schujman, Semiconducting ge clathrates: Promising candidates for thermoelectric applications, Applied Physics Letters **73**, 178 (1998).

[45] M. Christensen, A. B. Abrahamsen, N. B. Christensen, F. Juranyi, N. H. Andersen, K. Lefmann, J. Andreasson, C. R. Bahl, and B. B. Iversen, Avoided crossing of rattler modes in thermoelectric materials, Nature materials **7**, 811 (2008).

[46] J. Dong, O. F. Sankey, and C. W. Myles, Theoretical study of the lattice thermal conductivity in ge framework semiconductors, Physical review letters **86**, 2361 (2001).

[47] R. Wei, G. Huiyuan, Z. Zihao, and Z. Lixia, Filling-fraction fluctuation leading to glasslike ultralow thermal conductivity in caged skutterudites, Physical Review Letters **118**, 245901 (2017).

[48] B. Sales, D. Mandrus, and R. K. Williams, Filled skutterudite antimonides: A new class of thermoelectric materials, Science **272**, 1325 (1996).

[49] G. Meisner, D. Morelli, S. Hu, J. Yang, and C. Uher, Structure and lattice thermal conductivity of fractionally filled skutterudites: Solid solutions of fully filled and unfilled end members, Physical Review Letters **80**, 3551 (1998).

[50] H. Lin, G. Tan, J.-N. Shen, S. Hao, L.-M. Wu, N. Calta, C. Malliakas, S. Wang, C. Uher, C. Wolverton, and M. G. Kanatzidis, Concerted rattling in $CsAg_5Te_3$ leading to ultralow thermal conductivity and high thermoelectric performance, Angewandte Chemie **128**, 11603 (2016).

[51] T. Lanigan-Atkins, X. He, M. Krogstad, D. Pajerowski, D. Abernathy, G. N. Xu, Z. Xu, D.-Y. Chung, M. Kanatzidis, S. Rosenkranz, *et al.*, Two-dimensional overdamped fluctuations of the soft perovskite lattice in cspbbr3, Nature materials **20**, 977 (2021).

[52] N. J. Weadock, T. C. Sterling, J. A. Vigil, A. Gold-Parker, I. C. Smith, B. Ahammed, M. J. Krogstad, F. Ye, D. Voneshen, P. M. Gehring, *et al.*, The nature of dynamic local order in ch3nh3pbi3 and ch3nh3pbbr3, Joule **7**, 1051 (2023).

[53] W. J. Baldwin, X. Liang, J. Klarbring, M. Dubajic, D. Dell'Angelo, C. Sutton, C. Caddeo, S. D. Stranks, A. Mattoni, A. Walsh, *et al.*, Dynamic local structure in caesium lead iodide: spatial correlation and transient domains, Small **20**, 2303565 (2024).

[54] A. Mattoni, A. Filippetti, M. Saba, and P. Delugas, Methylammonium rotational dynamics in lead halide perovskite by classical molecular dynamics: The role of temperature, The Journal of Physical Chemistry C **119**, 17421 (2015).

[55] T. Hata, G. Giorgi, K. Yamashita, C. Caddeo, and A. Mattoni, Development of a classical interatomic potential for mapbbr3, The Journal of Physical Chemistry C **121**, 3724 (2017).

[56] A. Giri, S. Thakur, and A. Mattoni, Molecular rotor–rotor heat diffusion at the origin of the enhanced thermal conductivity of hybrid perovskites at high temperatures, Chemistry of Materials (2022).

[57] M. Wang and S. Lin, Anisotropic and ultralow phonon thermal transport in organic–inorganic hybrid perovskites: Atomistic insights into solar cell thermal management and thermoelectric energy conversion efficiency, Advanced Functional Materials **26**, 5297 (2016).

[58] A. Giri, A. Z. Chen, A. Mattoni, K. Aryana, D. Zhang, X. Hu, S.-H. Lee, J. J. Choi, and P. E. Hopkins, Ultralow thermal conductivity of two-dimensional metal halide perovskites, Nano letters **20**, 3331 (2020).

[59] C. Caddeo, C. Melis, M. I. Saba, A. Filippetti, L. Colombo, and A. Mattoni, Tuning the thermal conductivity of methylammonium lead halide by the molecular substructure, Physical Chemistry Chemical Physics **18**, 24318 (2016).

[60] C. Caddeo, A. Filippetti, and A. Mattoni, The dominant role of surfaces in the hysteretic behavior of hybrid perovskites, Nano Energy **67**, 104162 (2020).

[61] A. Mattoni and C. Caddeo, Dielectric function of hybrid perovskites at finite temperature investigated by classical molecular dynamics, The Journal of Chemical Physics **152**, 104705 (2020).

[62] M. A. Rahman and A. Giri, Uniquely anisotropic mechanical and thermal responses of hybrid organic–inorganic perovskites under uniaxial strain, The Journal of Chemical Physics **155**, 124703 (2021).

[63] A. Mattoni, A. Filippetti, M. Saba, C. Caddeo, and P. Delugas, Temperature evolution of methylammonium trihalide vibrations at the atomic scale, The Journal of Physical Chemistry Letters **7**, 529 (2016).

[64] P. Delugas, C. Caddeo, A. Filippetti, and A. Mattoni, Thermally activated point defect diffusion in methylammonium lead trihalide: Anisotropic and ultrahigh mobility of iodine, The journal of physical chemistry letters **7**, 2356 (2016).

[65] B. Thomas, N. Marks, and B. Begg, Developing pair potentials for simulating radiation damage in complex oxides, Nuclear Instruments and Methods in Physics Research Section B: Beam Interactions with Materials and Atoms **228**, 288 (2005).

[66] N. A. Benedek, A. L.-S. Chua, C. Elsässer, A. P. Sutton, and M. W. Finnis, Interatomic potentials for strontium titanate: An assessment of their transferability and comparison with density functional theory, Physical Review B—Condensed Matter and Materials Physics **78**, 064110 (2008).

[67] S. Thakur and A. Giri, Origin of ultralow thermal conductivity in metal halide perovskites, ACS Applied Materials & Interfaces **15**, 26755 (2023).

[68] S. Plimpton, Fast parallel algorithms for short-range molecular dynamics, Journal of computational physics **117**, 1 (1995).

[69] W. G. Hoover, Canonical dynamics: Equilibrium phase-space distributions, Physical review A **31**, 1695 (1985).

[70] A. P. Thompson, S. J. Plimpton, and W. Mattson, General formulation of pressure and stress tensor for arbitrary many-body interaction potentials under periodic boundary conditions, The Journal of chemical physics **131**, 154107 (2009).

[71] P. Brown, A. Fox, E. Maslen, M. O'keefe, and B. Willis, 6.1. intensity of diffracted intensities, International Tables for Crystallography C **554** (2006).

[72] T. F. Harrelson, M. Dettmann, C. Scherer, D. Andrienko, A. J. Moulé, and R. Faller, Computing inelastic neutron scattering spectra from molecular dynamics trajectories, Scientific reports **11**, 7938 (2021).

[73] G. L. Squires, *Introduction to the theory of thermal neutron scattering* (Courier Corporation, 1996).

[74] L. Van Hove, Correlations in space and time and born approximation scattering in systems of interacting particles, Physical Review **95**, 249 (1954).

[75] S. Xiong, D. Selli, S. Neogi, and D. Donadio, Native surface oxide turns alloyed silicon membranes into nanophononic metamaterials with ultralow thermal conductivity, Physical Review B **95**, 180301 (2017).

[76] T. Zushi, K. Ohmori, K. Yamada, and T. Watanabe, Effect of a sio 2 layer on the thermal transport properties of¡ 100¿ si nanowires: A molecular dynamics study, Physical Review B **91**, 115308 (2015).

[77] J. A. Thomas, J. E. Turney, R. M. Iutzi, C. H. Amon, and A. J. McGaughey, Predicting phonon dispersion relations and lifetimes from the spectral energy density, Physical Review B **81**, 081411 (2010).

[78] J. A. Thomas, J. E. Turney, R. M. Iutzi, C. H. Amon, and A. J. McGaughey, Erratum: Predicting phonon dispersion relations and lifetimes from the spectral energy density [Phys. Rev. B 81, 081411 (R)(2010)], Physical Review B **91**, 239905 (2015).

[79] T. Feng, B. Qiu, and X. Ruan, Anharmonicity and necessity of phonon eigenvectors in the phonon normal mode analysis, Journal of Applied Physics **117** (2015).

[80] K. Sääskilahti, J. Oksanen, J. Tulkki, and S. Volz, Role of anharmonic phonon scattering in the spectrally decomposed thermal conductance at planar interfaces, Physical Review B **90**, 134312 (2014).

[81] D. G. Cahill, S. K. Watson, and R. O. Pohl, Lower limit to the thermal conductivity of disordered crystals, Physical Review B **46**, 6131 (1992).

[82] Y. Zhao, S. Zeng, G. Li, C. Lian, Z. Dai, S. Meng, and J. Ni, Lattice thermal conductivity including phonon frequency shifts and scattering rates induced by quartic anharmonicity in cubic oxide and fluoride perovskites, Physical Review B **104**, 224304 (2021).

[83] T. Maekawa, K. Kurosaki, and S. Yamanaka, Thermal and mechanical properties of perovskite-type barium hafnate, Journal of alloys and compounds **407**, 44 (2006).

[84] S. Yamanaka, T. Hamaguchi, T. Oyama, T. Matsuda, S.-i. Kobayashi, and K. Kurosaki, Heat capacities and thermal conductivities of perovskite type bazro3 and baceo3, Journal of alloys and compounds **359**, 1 (2003).

[85] Z. Tong, Y. Zhang, A. Pecchia, C. Yam, L. Zhou, T. Dumitrică, and T. Frauenheim, Predicting the lattice thermal conductivity in nitride perovskite lawn3 from ab initio lattice dynamics, Advanced Science **10**, 2205934 (2023).

[86] M. Tachibana, T. Kolodiazhnyi, and E. Takayama-Muromachi, Thermal conductivity of perovskite ferroelectrics, Applied Physics Letters **93** (2008).

[87] E. Osei-Agyemang, C. E. Adu, and G. Balasubramanian, Ultralow lattice thermal conductivity of chalcogenide perovskite cazrse3 contributes to high thermoelectric figure of merit, npj Computational Materials **5**, 116 (2019).

[88] B. Sun, S. Niu, R. P. Hermann, J. Moon, N. Shulumba, K. Page, B. Zhao, A. S. Thind, K. Mahalingam, J. Milam-Guerrero, *et al.*, High frequency atomic tunneling yields ultralow and glass-like thermal conductivity in chalcogenide single crystals, Nature Communications **11**, 6039 (2020).

[89] Y. He, C. C. Stoumpos, I. Hadar, Z. Luo, K. M. McCall, Z. Liu, D. Y. Chung, B. W. Wessels, and M. G. Kanatzidis, Demonstration of energy-resolved γ-ray detection at room temperature by the cspbcl3 perovskite semiconductor, Journal of the American Chemical Society **143**, 2068 (2021).

[90] C. Kittel, Introduction to solid state physics, 6th edn., translated by y, Uno, N. Tsuya, A. Morita and J. Yamashita,(Maruzen, Tokyo, 1986) pp , 124 (1986).

[91] P. Klemens, The scattering of low-frequency lattice waves by static imperfections, Proceedings of the Physical Society. Section A **68**, 1113 (1955).

[92] See Supplemental Material at [URL will be inserted by publisher] for additional details including phonon dispersion calculations, calculations of bulk and Young's moduli, X-ray diffraction patterns, analysis of the temperature dependence of thermal conductivity in relation to phase transitions, vibrational density of states, mean square displacements, atomic probability distributions, supplementary neutron diffuse scattering results, and the nudged elastic band (NEB) calculations. The Supplemental Material also contains Refs. [115–117].

[93] W. Li and N. Mingo, Thermal conductivity of fully filled skutterudites: Role of the filler, Physical Review B **89**, 184304 (2014).

[94] V. M. Nield and D. A. Keen, *Diffuse neutron scattering from crystalline materials*, Vol. 14 (Oxford University Press, 2001).

[95] M. Carignano, Y. Saeed, S. A. Aravindh, I. S. Roqan, J. Even, and C. Katan, A close examination of the structure and dynamics of hc (nh 2) 2 pbi 3 by md simulations and group theory, Physical Chemistry Chemical Physics **18**, 27109 (2016).

[96] X.-G. Zhao, G. M. Dalpian, Z. Wang, and A. Zunger, Polymorphous nature of cubic halide perovskites, Physical Review B **101**, 155137 (2020).

[97] M. Zacharias, G. Volonakis, F. Giustino, and J. Even, Anharmonic electron-phonon coupling in ultrasoft and locally disordered perovskites, npj Computational Materials **9**, 153 (2023).

[98] F. Ke, C. Wang, C. Jia, N. R. Wolf, J. Yan, S. Niu, T. P. Devereaux, H. I. Karunadasa, W. L. Mao, and Y. Lin, Preserving a robust cspbi3 perovskite phase via pressure-directed octahedral tilt, Nature communications **12**, 461 (2021).

[99] J. A. Steele, H. Jin, I. Dovgaliuk, R. F. Berger, T. Braeckevelt, H. Yuan, C. Martin, E. Solano, K. Lejaeghere, S. M. Rogge, *et al.*, Thermal unequilibrium of strained black cspbi3 thin films, Science **365**, 679 (2019).

[100] A. Jaffe, Y. Lin, and H. I. Karunadasa, Halide perovskites under pressure: accessing new properties through lattice compression, ACS Energy Letters **2**, 1549 (2017).

[101] A. Jaffe, Y. Lin, C. M. Beavers, J. Voss, W. L. Mao, and H. I. Karunadasa, High-pressure single-crystal structures of 3d lead-halide hybrid perovskites and pressure effects on their electronic and optical properties, ACS Central Science **2**, 201 (2016).

[102] J. Li, M. Bouchard, P. Reiss, D. Aldakov, S. Pouget, R. Demadrille, C. Aumaitre, B. Frick, D. Djurado, M. Rossi, *et al.*, Activation energy of organic cation rotation in ch3nh3pbi3 and cd3nh3pbi3: quasi-elastic neutron scattering measurements and first-principles analysis including nuclear quantum effects, The journal of physical chemistry letters **9**, 3969 (2018).

[103] A. M. Leguy, J. M. Frost, A. P. McMahon, V. G. Sakai, W. Kockelmann, C. Law, X. Li, F. Foglia, A. Walsh, and B. C. O'regan, The dynamics of methylammonium ions in hybrid organic–inorganic perovskite solar cells, Nature communications **6**, 7124 (2015).

[104] G. Henkelman and H. Jónsson, Improved tangent estimate in the nudged elastic band method for finding minimum energy paths and saddle points, The Journal of Chemical Physics **113**, 9978 (2000).

[105] G. Henkelman, B. P. Uberuaga, and H. Jónsson, A climbing image nudged elastic band method for finding saddle points and minimum energy paths, The Journal of Chemical Physics **113**, 9901 (2000).

[106] G.-Y. Chen, Z.-D. Guo, X.-G. Gong, and W.-J. Yin, Kinetic pathway of γ-to-δ phase transition in cspbi3, Chem **8**, 3120 (2022).

[107] J. Klarbring, Low-energy paths for octahedral tilting in inorganic halide perovskites, Physical Review B **99**, 104105 (2019).

[108] T. Feng and X. Ruan, Quantum mechanical prediction of four-phonon scattering rates and reduced thermal conductivity of solids, Physical Review B **93**, 045202 (2016).

[109] T. Feng, L. Lindsay, and X. Ruan, Four-phonon scattering significantly reduces intrinsic thermal conductivity of solids, Physical Review B **96**, 161201 (2017).

[110] T. Feng and X. Ruan, Four-phonon scattering reduces intrinsic thermal conductivity of graphene and the contributions from flexural phonons, Physical Review B **97**, 045202 (2018).

[111] M. Dubajic, J. R. Neilson, J. Klarbring, X. Liang, S. A. Boer, K. C. Rule, J. E. Auckett, L. Gu, X. Jia, A. Pusch, *et al.*, Dynamic nanodomains dictate macroscopic properties in lead halide perovskites, arXiv preprint arXiv:2404.14598 (2024).

[112] C. Ge, M. Hu, P. Wu, Q. Tan, Z. Chen, Y. Wang, J. Shi, and J. Feng, Ultralow thermal conductivity and ultrahigh thermal expansion of single-crystal organic–inorganic hybrid perovskite $CH_3NH_3PbX_3$ (X= Cl, Br, I), The Journal of Physical Chemistry C **122**, 15973 (2018).

[113] T. Handa, T. Yamada, M. Nagai, and Y. Kanemitsu, Phonon, thermal, and thermo-optical properties of halide perovskites, Physical Chemistry Chemical Physics **22**, 26069 (2020).

[114] P. B. Allen and J. L. Feldman, Thermal conductivity of glasses: Theory and application to amorphous si, Physical review letters **62**, 645 (1989).

[115] T. Tadano, Y. Gohda, and S. Tsuneyuki, Anharmonic force constants extracted from first-principles molecular dynamics: applications to heat transfer simulations, Journal of Physics: Condensed Matter **26**, 225402 (2014).

[116] F. D. Murnaghan, The compressibility of media under extreme pressures, Proceedings of the National Academy of Sciences **30**, 244 (1944).

[117] V. Tyuterev and N. Vast, Murnaghan's equation of state for the electronic ground state energy, Computational materials science **38**, 350 (2006).